THESIS FOR THE DEGREE OF LICENTIATE OF ENGINEERING

PEM fuel cell temperature management for high performance

Christian Boßer

Department of Mechanics and Maritime Sciences

CHALMERS UNIVERSITY OF TECHNOLOGY

Gothenburg, Sweden 2025

PEM fuel cell temperature management for high performance

Christian Boßer

Licentiateavhandlingar vid Chalmers tekniska högskola

Department of Mechanics and Maritime Sciences

Chalmers University of Technology

SE-412 96 Gothenburg

Sweden

Telephone + 46 (0)31-772 1000

Cover: Project overview - Heavy-duty fuel cell truck simulation model to develop improved cooling solutions with experimental validation of cooling systems and fuel cell models

Illustration by Christian Boßer

Printed by Chalmers Digitaltryck

Gothenburg, Sweden 2025

Abstract

PEM fuel cell temperature management for high performance
Christian Boßer
Department of Mechanics and Maritime Sciences
Division of Transport, Energy and Environment
Chalmers University of Technology

Addressing the thermal management challenges of low-temperature proton exchange membrane fuel cells (PEMFCs) is an important step to enable the decarbonization of heavy-duty transport with hydrogen as a fuel. Due to the low operating temperature of 60-90°C, PEMFC vehicles require large radiators to achieve sufficient heat rejection which makes alternative cooling solutions desirable. Other key challenges in the development of PEMFC like lifetime and cost are also significantly impacted by the thermal management system.

The presented project is part of a holistic approach to address thermal management and lifetime challenges in heavy-duty fuel cell vehicles. First a verified 0D/1D heavy-duty truck vehicle model with conventional cooling system has been developed to identify its thermal limitations and the resulting impact on the vehicle performance. Already at 20°C ambient temperature, severe thermal limitations require a PEMFC performance reduction of up to 46% to prevent overheating in the hill climb scenario investigated in this work. Integrating components like a braking resistor to substitute engine braking in the vehicle model shows that thermal management not only impacts the vehicle performance during uphill but also downhill driving. The identification of these limitations enabled the design of a highly integrated bubble column evaporative cooling solution that utilizes the PEMFC product water complementary to the established radiator cooling system. The project focus is on worst-case cooling conditions of high fuel cell load and elevated ambient temperatures. A collaborative development of an enhanced fuel cell model shall eventually allow for a detailed evaluation of the interdependency of thermal management, vehicle performance, degradation, fuel cell operation and auxiliary equipment over the lifetime of a vehicle. Moreover, the modular structure allows for the integration of these solutions in other heavy-duty vehicles.

This thesis presents a complementary technical background to the investigations done thus far. The results of the publications within this project are summarized and an overview of the planned future work is presented.

Keywords: PEMFC, Thermal management, Heavy-duty, Vehicle model, Cooling system, Evaporative cooling, Bubble column, Hydrogen

Acknowledgment

First and foremost, I want to thank my supervisor Prof. David Sedarsky for the guidance and for discussing all of my ideas and our fuel cell projects at large. Giving me the freedom to not only think about and model but also build and test my ideas makes the project fun and rewarding.

I also want to thank all the colleagues involved in the development of the simulation models and experimental setups. Especially, I want to thank Gustavo Hindi from Volvo Trucks for the support on the truck vehicle model and everyone involved in our TechForH2 fuel cell reference group. For the support with the prototype test bench, I want to thank the lab and research engineers at the Department of Mechanics and Maritime Sciences at Chalmers University, especially Robert Buadu, Isak Jonsson, Valentin Vikhorev and Prof. Valery Chernoray.

Furthermore, I would like to thank the all partners in the TechForH2 Competence Centre for financially supporting this project. The Competence Centre TechForH2 is hosted by Chalmers University of Technology and is financially supported by the Swedish Energy Agency (P2021-90268) and the member companies Volvo, Scania, Siemens Energy, GKN Aerospace, PowerCell, Oxeon, RISE, Stena Rederier AB, Johnson Matthey and Insplorion.

Of course, I also want to thank all colleagues at (now) the divisions of Transport, Energy and Environment as well as Fluid Dynamics, especially the junior researchers that make the workdays, after-works and weekends in Gothenburg fun.

Finally, I want to thank my family and friends in various parts of the world for supporting me throughout the project and despite the distance from home.

Christian Boßer

Göteborg, May 2025

List of publications

This thesis is based on the work contained in the following appended publications:

Paper I

C. Boßer and D. Sedarsky, “BUBBLE COLUMN EVAPORATIVE COOLING FOR PEMFC THERMAL MANAGEMENT IN HEAVY-DUTY VEHICLES,” presented at the 10th Thermal and Fluids Engineering Conference (TFEC), Begel House Inc., 2025. doi: 10.1615/TFEC2025.mes.055991.

Paper II (Submitted manuscript)

C. Boßer and D. Sedarsky, “Verified PEM fuel cell heavy-duty long-haul truck vehicle model with thermal management limitations of conventional cooling systems”, submitted manuscript, 2025

Paper III (Submitted manuscript)

C. Boßer and D. Sedarsky, “Evaporative bubble column cooling for PEMFC heavy-duty vehicle thermal management with experimental proof-of-concept”, submitted manuscript, 2025

List of additional publications and reports

Conference presentation I

C. Boßer and D. Sedarsky, Presentation: *Ammonia sorption heat pump for PEM fuel cell thermal management in heavy duty transport*, presented at the 8th Thermal and Fluids Engineering Conference (TFEC), March 26-29, 2023

Contents

Nomenclature

Abbreviations

AHT	**A**bsorption **h**eat **t**ransformer
BoP	**B**alance **o**f **p**lant
BPP	**Bip**olar **p**late
CL	**C**atalyst **l**ayer
COP	**C**oefficient **o**f **p**erformance
FC	**F**uel **c**ell
FCEV	**F**uel **c**ell **e**lectric **v**ehicle
FCS	**F**uel **c**ell **s**ystem
GDL	**G**as **d**iffusion **l**ayer
GHG	**G**reen**h**ouse **g**as
HD	**H**eavy-**d**uty
HHV	**H**igher **h**eating **v**alue
HOR	**H**ydrogen **o**xidation **r**eaction
HT	**H**igh **t**emperature
LHV	**L**ower **h**eating **v**alue
LT	**L**ow **t**emperature
MEA	**M**embrane **e**lectrode **a**ssembly
MPL	**M**icro **p**orous **l**ayer
MT	**M**edium **t**emperature
ORR	**O**xygen **r**eduction **r**eaction
PCM	**P**hase **c**hange **m**aterial
PEMFC	**P**roton **e**xchange **m**embrane **f**uel **c**ell
STP	**S**tandard **t**emperature and **p**ressure

Symbols

A	Area
c_d	Aerodynamic drag coefficient
c_p	Constant pressure specific heat capacity
COP	Coefficient of performance
E	Potential/voltage
f_r	Friction coefficient
F	Force
Δg_{rxn}	Gibbs free energy change of reaction
Gr	Grashof number
h	Convective heat transfer coefficient
Δh_{rxn}	Enthalpy change of reaction/enthalpy of reaction
Δh_v	Heat of vaporization
I	Current
k	Thermal conductivity
L	Wall/characteristic length
m	Mass
$\dot{m}$	Mass flow rate
n	Number of transferred electrons
NTU	Number of transfer units
Nu	Nusselt number
p	(Partial) pressure
Pr	Prandtl number
$\dot{Q}$	Heat flow rate
Re	Reynolds number

ΔS	Reaction entropy change
t	Time
T	Temperature
ΔT	Temperature drop/difference
U	Overall heat transfer coefficient
v	Velocity
V	Voltage
ΔV	Voltage drop

Greek symbols

α	Road slope
β	Thermal volume expansion coefficient
γ	Gear ratio
ε	Efficiency/effectiveness/radiative emissivity
Θ	Moment of inertia
μ	Dynamic viscosity
ρ	Density
φ	Relative humidity
ω	(Absolute) humidity ratio

Subscripts

0	Standard temperature and pressure
1,2,3,4	Separate (wall) surfaces/components
a	Air
A	Absorber
A, B, C	Separate (wall) segments
act	Activation
amb	Ambient
c	Cold
C	Condenser
$cell$	(Single) cell
$cnct$	Contact
$conc$	Concentration
$cond$	Conduction
$conv$	Convection
$drag$	Aerodynamic drag
dry	Dry (air)
E	Evaporator
$evap$	Evaporated
f	Fluid
$forced$	Forced (convection)
$free$	Free (convection)
$front$	Frontal (area)
G	Generator
gap	Gap
h	Hot
HHV	Higher heating value
$high$	High value
i	Inlet
lat	Latent
LHV	Lower heating value
lm	Logarithmic
low	Low value
max	Maximum value

min	Minimum value
o	Outlet
$ohmic$	Ohmic
p	Powertrain
$pump$	Pump
r	Rotating
rad	Radiative
$roll$	Rolling
s	Surface
sat	Saturation (pressure)
$slope$	Road slope
sur	Surroundings
t	total
$thermo$	Thermodynamic
$trac$	Traction
v	Vapor
veh	Vehicle
w	Wall/water/wheel

Superscripts

0	Standard temperature and pressure
H	Thermoneutral

Constants

F	Faraday's constant = 96,485 C/mol
g	Gravitational acceleration = 9.81 m/s²
R	Ideal gas constant = 8.314 J/(mol K)
σ	Stefan-Boltzmann constant = $5.67 \cdot 10^{-8}$ W/(m²K⁴)

Physics/chemistry symbols

e^-	Electron
H_2	Hydrogen
H^+	Proton
H_2O	Water
Li	Lithium
$LiBr$	Lithium bromide
$LiNO_3$	Lithium nitrate
NH_3	Ammonia
O_2	Oxygen

List of Figures

Chapter 1

Introduction

In the following thesis, the investigations thus far conducted in the "PEM fuel cell temperature management for high performance" project are presented. The project aims to enhance the understanding of thermal limitations in heavy-duty vehicles with state-of-the-art low-temperature proton-exchange membrane fuel cells and how to overcome them. First, in chapter 1 the motivation, approach and outline of the project are presented. An overview of the technical background is presented in chapter 2, followed by a summary of the publications in chapter 3 and finally, the conclusion and future work in chapter 4.

1.1 Motivation

This project is driven by the aim to support the development of sustainable transport, in particular the reduction of greenhouse gas (GHG) emissions from heavy-duty (HD) vehicles. As shown in Figure 1, the impact of the road transport sector on the total GHG emissions of the EU is significant and a large share caused by HD vehicles, i.e. HD-trucks, trains, planes and ships.

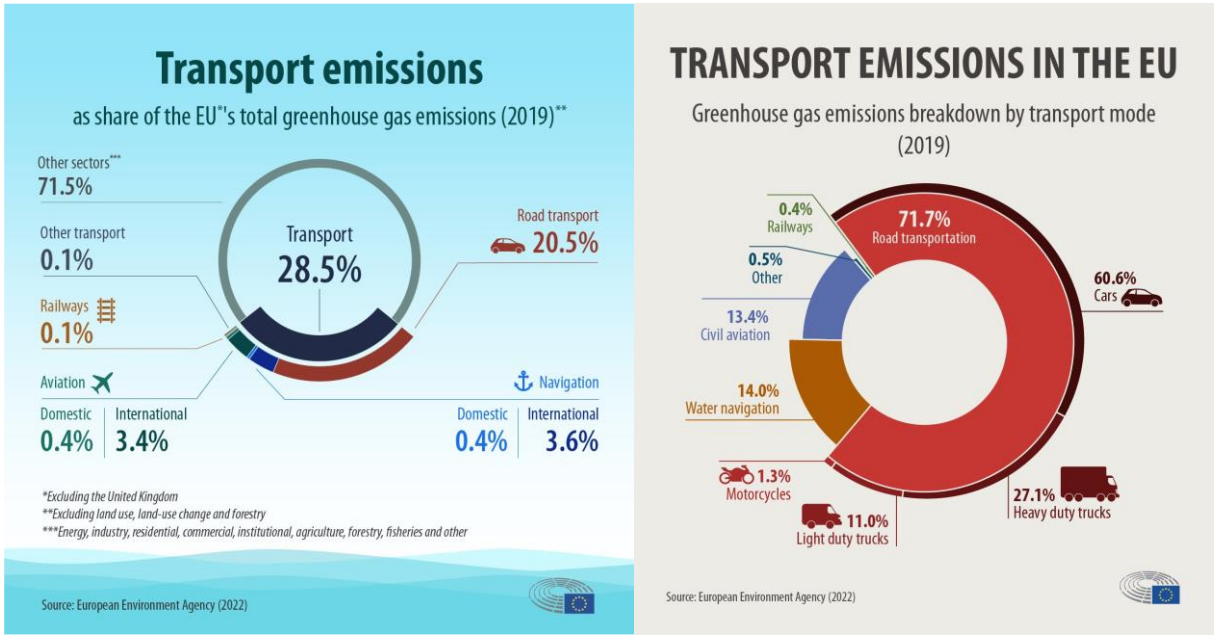

Figure 1: Greenhouse gas emissions of the transport sector in the EU and breakdown by transport mode (2019) [1-2]

The main focus of the project is on HD trucks, which are responsible for a large share of the transport emissions and from which the developed solutions shall be transferred to other modes of HD transport. Electrifying HD vehicles with proton exchange membrane fuel cells (PEMFCs) leverages their

advantages of high efficiency, power density, quiet operation, zero tailpipe emissions and short start-up times. Compared to battery electric trucks that require heavy and large battery packs that can significantly impact the payload capacity, fuel cell electric vehicles (FCEVs) can achieve long driving distances with short refueling times, although the low density of hydrogen leads to large tank systems [3-7].

In comparison to the PEMFC systems developed for passenger cars, HD trucks are more cost sensitive and have higher requirements in the form of higher target peak efficiencies of 68% (2030) as well as increased lifetime and milage expectations of over 25,000 h or 1 million miles (2030), respectively. While peak FC system efficiencies today almost reach these targets with efficiencies of 60-65% at low loads, efficiencies decrease to about 45% at rated power, leading to high heat loads of roughly the same the level as the gross power production. The typical operation at high loads on highways increases the demand on the thermal management systems. Thus, key challenges are identified as the reduction of costs and parasitic power consumption, improved durability and thermal management [3], [4], [5], [8], [9].

1.2 Approach and outline of the thesis

The aim of the project is to identify and quantify the thermal limitations of state-of-the-art HD PEMFC vehicles and to develop solutions to overcome these. To achieve this goal, a multiphysics vehicle level 0D/1D simulation approach has been applied to model the relevant processes ranging from electrochemical reactions in the FC to the required traction power of the vehicle at low computational cost, an important advantage for the iterative development of FC systems [10]. The advantage of this approach lies in the possibility to incorporate the interdependences between the many components required in a FCEV and thus capture additional heat loads, parasitic power losses and details of the FC operation. Investigations are conducted on representative load profiles identified from driving cycles for typical operation and challenging scenarios like hill climbs and high ambient temperatures. An overview of the project is shown in the following Figure 2:

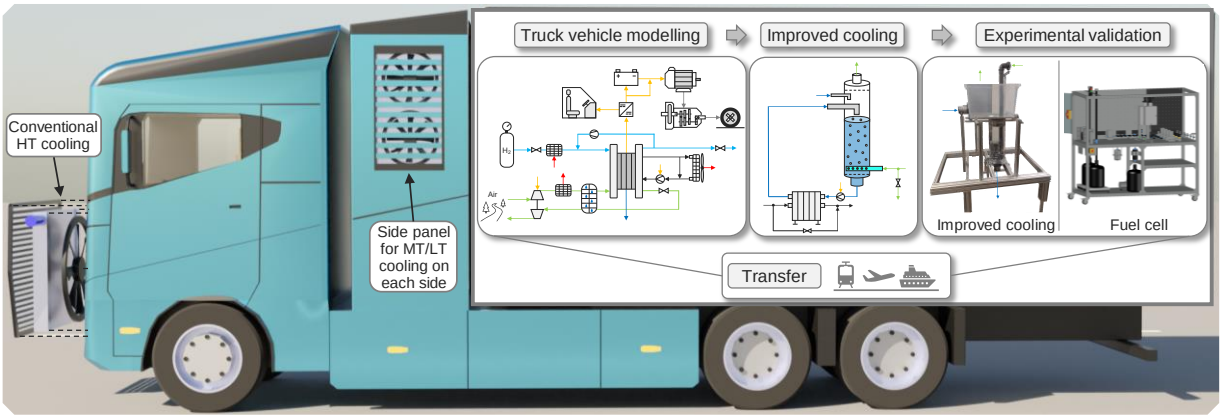

Figure 2: Project structure overview (HT, MT, LT: high, medium, low temperature)

The project's aim is to answer the following four research questions:

1) How can sufficient heat rejection be achieved to prevent overheating and to maintain the target FC temperature even in challenging conditions at high loads and elevated ambient temperatures?
2) What influence does the thermal management have on the operation of the FC and its performance over lifetime?
3) What is the impact of a potential cooling solution on the system efficiency?
4) Are the size, weight and cost requirement of this solution realizable in transport applications and competitive with alternative solutions?

Thus, in the first step a verified detailed 0D/1D HD FC truck vehicle model has been developed in Siemens Simcenter Amesim (2410) which includes often neglected aspects like the impact of braking resistors on the vehicle performance (Paper II). This vehicle model is the platform for the different projects of our reference group that address water management, lifetime, time response and thermal management. These projects are directly connected due to the interdependency of degradation, water and thermal management [10-11]. A modular structure of the vehicle and FCSs has been developed to integrate enhanced FC models and cooling solutions. The modular solutions can be adjusted to different HD applications in future steps. Thus, the developed vehicle model platform allows for the holistic investigation of the challenges that HD PEMFC vehicles face.

The contribution of this project to these advancements thus far are the development of the baseline truck vehicle model with conventional cooling system at beginning of life (BoL) conditions, its verification and the identification of its thermal limitations in Paper II. The developed model will be used to further analyze these thermal limitations. From these insights, a bubble column evaporative cooling concept has been developed to provide sufficient heat rejection even in challenging operating conditions, presented theoretically in Paper I and extended by proof-of-concept measurements in Paper III. To further investigate this solution and integrate it into the vehicle model is the focus for the remainder of the project. Additionally, principal methods for enhanced modular and spatially resolved single cell and stack models have been developed with emphasis on the overall heat transfer. To refine those models and experimentally validate them will enhance the analysis of the impact that the cooling system has on the FC operation.

Excluded from the scope of this project are cold climate conditions, packaging, component sizing, flow field design, energy management and drive train optimization studies. This includes investigation of predictive control with prior route information or how to package more radiators on a vehicle. The focus is set on a robust operation of the vehicle in thermally challenging driving scenarios. Hence, the developed vehicle model provides an academic platform for these investigations in future projects, e.g. to investigate the benefits of prior route information.

Chapter 2

Technical background

In the following chapter, the technical background of proton exchange membrane fuel cells is presented in section 2.1, followed by heat transfer including heat exchangers in section 2.2, fuel cell thermal management in section 2.3 and finally, longitudinal vehicle dynamics in section 2.4.

2.1 Proton exchange membrane fuel cells

In a fuel cell, chemically stored energy of a fuel is electrochemically converted to useable electrical energy [4]. Many different types of fuel cells exist, classified e.g. by the electrolyte, operating temperature or charge carrier. Overviews of different FC types are provided e.g. in [4] and [12]. The focus of this project is on low-temperature PEMFCs that operate between 60-90°C which is the most suitable for transportation applications today because of its high power density and efficiency [3-6].

In the case of PEMFCs, the energy is extracted from high purity hydrogen, which typically is an energy carrier produced from a primary energy source. The production of hydrogen is divided into many different categories depending on the origin of the hydrogen or source of energy to produce it. Significant losses exist in the production and supply chain of hydrogen and the potential (indirect) global warming impact of hydrogen needs to be considered. Production, supply, storage and environmental impact of hydrogen will not be further considered, more details can be found e.g. in [4], [6], [12] and [13]. In the following section 2.1.1 an overview of the fundamental working principle and structure of PEMFCs is presented, followed by the principles of forming a FC stack in section 2.1.2 and the necessary auxiliary components for an integrated fuel cell system (FCS) in section 2.1.3.

2.1.1 Working principle

The fundamental reaction in a PEMFC is the heat releasing exothermic formation of water from hydrogen and oxygen [4]:

$$H_2 + \frac{1}{2} O_2 \rightarrow H_2O \tag{1}$$

In a fuel cell, the reactants are spatially separated by an electrolyte which leads to individual pathways for the electrons and protons (H^+). This exchange of protons through the electrolyte gives PEMFCs their name. Protons and electrons are freed from hydrogen and react with oxygen according to the following half reactions [4]:

$$H_2 \leftrightharpoons 2H^+ + 2e^- \tag{2}$$

$$\frac{1}{2}O_2 + 2H^+ + 2e^- \leftrightharpoons H_2O \quad (3)$$

Half reaction (2) is called hydrogen oxidation reaction (HOR) and half reaction (3) oxygen reduction reaction (ORR). The basic structure of a PEM fuel cell is shown in the following schematic in Figure 3:

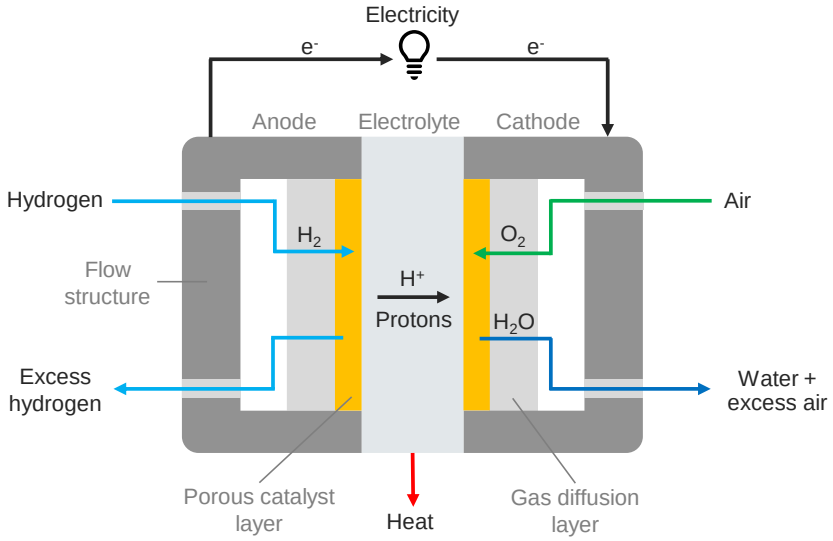

Figure 3: Schematic structure of a PEM fuel cell, adapted from [4]

In the basic FC principle shown in Figure 3, hydrogen is supplied through flow structures on the anode side where hydrogen splits into protons and electrons in the catalyst layer (CL). While the protons conduct through the electrolyte, the electrons are forced through the electric load by the potential difference between the electrodes, performing useable work. Thus, the operation of a FC requires an electrolyte that is conductive for ions but an insulator for electrons [4].

On the cathode side, oxygen is typically provided from air. Excess hydrogen and air flow out of the cell and the product water is removed by the excess air flow. A gas diffusion layer (GDL), often paired with an additional microporous layer (MPL), guides the reactant flow to the electrodes [4]. The electrodes (GDL, MPL, CL) and electrolyte (membrane) are summarized as the membrane electrode assembly (MEA) [12]. The majority of the produced heat is typically removed through cooling channels in the flow structure and only a small share through excess reactants. The electrodes and flow structures act as the current collectors and transfer the heat from the MEA to the cooling channels [4], [5], [11], [12]. Typical materials and requirements for the different components are further described in e.g. [3], [4] and [14].

The maximum electrical work that can be extracted from an isobaric and isothermal hydrogen-oxygen FC reaction is defined by the Gibbs free energy change of the reaction $\Delta\hat{g}^0_{rxn}$. At standard temperature and pressure (STP) with liquid product water, $\Delta\hat{g}^0_{rxn} = -237.2$ kJ/mol leads to a reversible voltage (E^0) defined as [4], [12]:

$$E^0 = \frac{\Delta\hat{g}^0_{rxn}}{n \cdot F} = 1.23\ V \quad (4)$$

with the number of moles of transferred electrons n (2 per mole H_2) and Faraday's constant $F = 96{,}485$ C/mol. While the reversible voltage defines the theoretical upper limit in a hydrogen-oxygen FC reaction, the thermoneutral voltage (E^H) defines the ideal cell voltage, determined from the enthalpy change of the hydrogen-oxygen reaction $\Delta\hat{h}^0_{rxn}$ (enthalpy of reaction). The enthalpy of reaction can be

evaluated with liquid or vapor product water, depending on the state in which water is produced in a particular FC. The difference between the respective enthalpies is the vaporization enthalpy of water that could theoretically be released and recovered by condensing the vapor. The two cases are called higher- (HHV) and lower heating value (LHV), respectively with the reaction enthalpies at STP of $\Delta\hat{h}^0_{rxn,HHV} = -285.8$ kJ/mol and $\Delta\hat{h}^0_{rxn,LHV} = -241.8$ kJ/mol. The thermoneutral voltage is defined as [4], [12]:

$$E^H = \frac{|\Delta\hat{h}^0_{rxn}|}{n \cdot F} \tag{5}$$

This results in a thermoneutral voltage of 1.48 V with HHV and 1.25 V with LHV. Assuming liquid product water in PEMFCs below 100°C, the theoretically achievable reversible thermodynamic efficiency (ε_{thermo}) at STP can be determined from the maximum electrical work and the total energy input [4], [12]:

$$\varepsilon_{thermo,HHV} = \frac{useful\ energy}{total\ energy} = \frac{\Delta\hat{g}^0_{rxn}}{\Delta\hat{h}^0_{rxn,HHV}} = 83\% \tag{6}$$

If not operated at STP, the reversible voltage changes depending on temperature, pressure and species concentration which is expressed as the Nernst potential (E), assuming ideal gases and liquid product water [4], [10]:

$$E = E^0 + \frac{\Delta S^0}{2F} \cdot (T - T_0) - \frac{R \cdot T}{2F} \cdot \ln \frac{1}{p_{H_2} \cdot p_{O_2}^{1/2}} \tag{7}$$

with the reaction entropy change $\Delta S^0 = 165$ J/(mol K), temperature T, STP temperature T_0, ideal gas constant $R = 8.314$ J/(mol K) and partial pressures p of hydrogen and oxygen. While increasing the pressure moderately increases the Nernst potential, increasing the temperature reduces it [4].

Besides these thermodynamic limitations of how much work can be extracted from a fuel, real FCs are subject to further irreversible losses. These are categorized into four voltage drops: (1) activation losses including fuel cross over and internal currents (ΔV_{act}), (2) ohmic losses (ΔV_{ohmic}) and (3) concentration losses (ΔV_{conc}). The resulting cell voltage (V_{cell}) can be determined as [4], [12]:

$$V_{cell} = E^0 - \Delta V_{act} - \Delta V_{ohmic} - \Delta V_{conc} \tag{8}$$

The polarization curve (cell voltage) can therefore also be interpreted as the cell efficiency. Thus, total heat loss ($\dot{Q}$) can be determined as the difference between the actual cell and thermoneutral voltage at a given current (I) [4], [12]:

$$\dot{Q} = (E^H - V_{cell}) \cdot I \tag{9}$$

The contribution of each voltage drop, total energy losses as well as the resulting power and heat production are schematically shown in the following Figure 4:

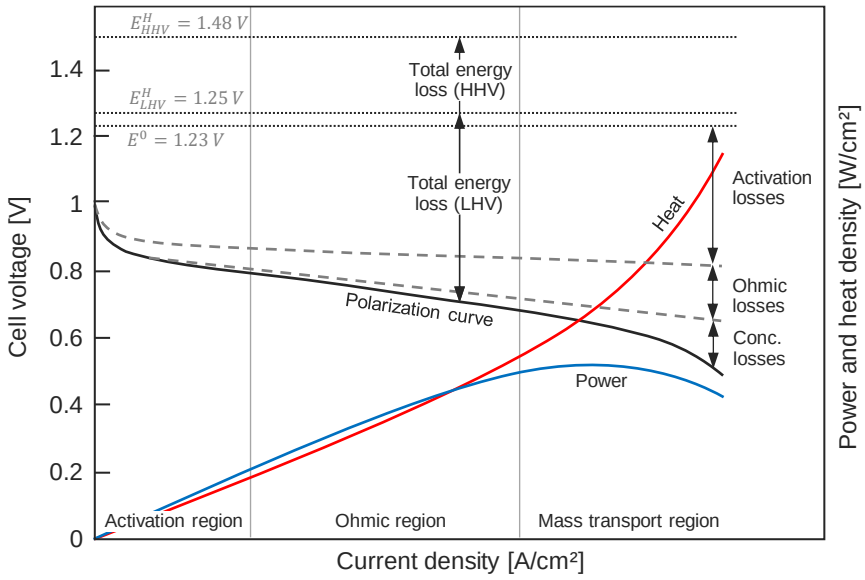

Figure 4: Schematic fuel cell voltage, power and heat curves including loss contributions at STP, adapted from [4], [5], [12], [15], [16]

The activation losses are defined by the reaction kinetics, i.e. how fast the reactions take place and thus how much current is produced. To reduce the necessary activation energy, catalysts are used and for the hydrogen-oxygen reaction in PEMFCs, platinum is the most suitable. These reactions take place at the triple phase boundary layer in the porous catalyst layer. The triple phase boundary layer is the contact between the ionomer, carbon and catalyst to allow for (1) contact between catalyst and reactant, (2) conduction of electrons to the carbon and (3) conduction of the protons through the ionomer into the membrane. Degradation effects like platinum particle growth or dissolution and carbon corrosion accelerate with voltage cycling and temperature. Platinum poisoning occurs from carbon monoxide or sulfur in the reactant supply [4], [12].

In a hydrogen-oxygen FC, the anode HOR is fast compared to the sluggish cathode ORR which therefore limits the overall reaction rate and causes the majority of the activation loss. In addition to using a catalyst, further aspects can reduce the activation losses: (1) Increasing the available reaction sites by increasing the surface area and catalyst loading. (2) Increasing the temperature increases the thermal energy of the reactants and thus the chance to overcome the activation barrier. And (3), while increasing the concentration of reactants by increasing the FC pressure only leads to small increases in the Nernst potential, the impact on the reaction kinetics is significant. Further details on kinetics, catalysis and how to model the activation losses with the Butler-Volmer or Tafel equation can be found e.g. in [4] and [12]. Additional to the activation losses, the FC voltage gets reduced by the crossover of hydrogen through the membrane, the generation of internal currents and side reactions [4], [12].

The ohmic voltage drop is caused by the conduction of electrons in the current collectors and ions in the electrolyte, leading to resistive heat losses in these components. Typically, ion conductivity has a larger impact, thus the thickness of the membrane needs to be balanced to reduce ohmic losses while providing sufficient mechanical strength and avoiding increased fuel crossover. In PEMFCs, typically solid polymer thin film membranes like Nafion™ are used and require a certain water content for ion conduction. This water content needs to be ensured by sufficient humidification through the reactant supply and is critical for the ohmic losses and lifetime of the membrane. Ensuring sufficient water management and membrane temperatures below 100°C is crucial for the performance of PEMFCs since high temperatures lead to drying of the membrane. Higher FC pressures reduce the necessary amount of water content in the inlet air to achieve high relative humidities and are therefore beneficial for the water

management (see section 2.2.3). Degradation occurs from chemical effects like free radicals and ion contamination and mechanical damage and stresses caused by temperature and humidity cycling [4], [12]. The sorption and desorption of water at membrane and GDL interfaces are an additional heat source or sink in the MEA [17]. Further details of ion transport mechanisms as well as modelling of ion conductivity and membrane humidification can be found e.g. in [4], [11] and [12].

Mass transport limitations are caused by insufficient reactant supply and product removal. Insufficient supply reduces the reactant concentration at the reaction sites in the CL and thus the FC performance. Deficits can arise from insufficient flow rates or non-uniform distribution in the flow channels, limited mass transfer from the flow channel into the electrodes and limitations in the diffusion rate through the porous electrodes. Limitations in product removal can be caused by liquid water that blocks flow channels or reduces the porosity of the electrodes and thus the mass transport. This effect is called flooding [4], [11], [12]. Further details on the channel flow and species diffusion limitations can be found e.g. in [4]. An additional non-uniformity arises from heat release and transfer within the MEA. As most of the heat is produced in the CL at the cathode side and the ohmic losses in the membrane, the temperature profile over the MEA can vary by several degrees. The heat transfer within the cell is not only impacted by the specific MEA materials but also the compression uniformity as well as water distribution and transport [5], [11], [18].

Furthermore, some hydrogen that is provided to the anode will flow out of the FC unreacted or contribute to side reactions and thus not to the desired electrochemical reaction. Typical fuel utilization efficiencies are around 95% and can generally be improved by surplus hydrogen supply. The ratio between the required and supplied amount of a reactant is called stoichiometry. Higher stoichiometries can lead to waste of fuel on the hydrogen side and higher parasitic power losses on the air side (see section 2.1.3). But higher stoichiometries on the air side reduce the concentration losses caused by the low oxygen concentration of 21% in air. An increased excess air flow can also remove more product water to prevent flooding [4], [12].

2.1.2 Fuel cell stack

To achieve sufficient power to propel a vehicle, multiple cells need to be connected to form a FC stack. Electrically connecting cells in series increases the total voltage at theoretically the same current in each cell. In multi-cell arrangements, bipolar plates (BPP) facilitate alternating flow channels for the anode, cathode and cooling channels, act as current collectors and provide structural support [4], [11], [12]. A cut-section of two FCs as part of a multi-cell arrangement and a full stack are schematically shown in Figure 5:

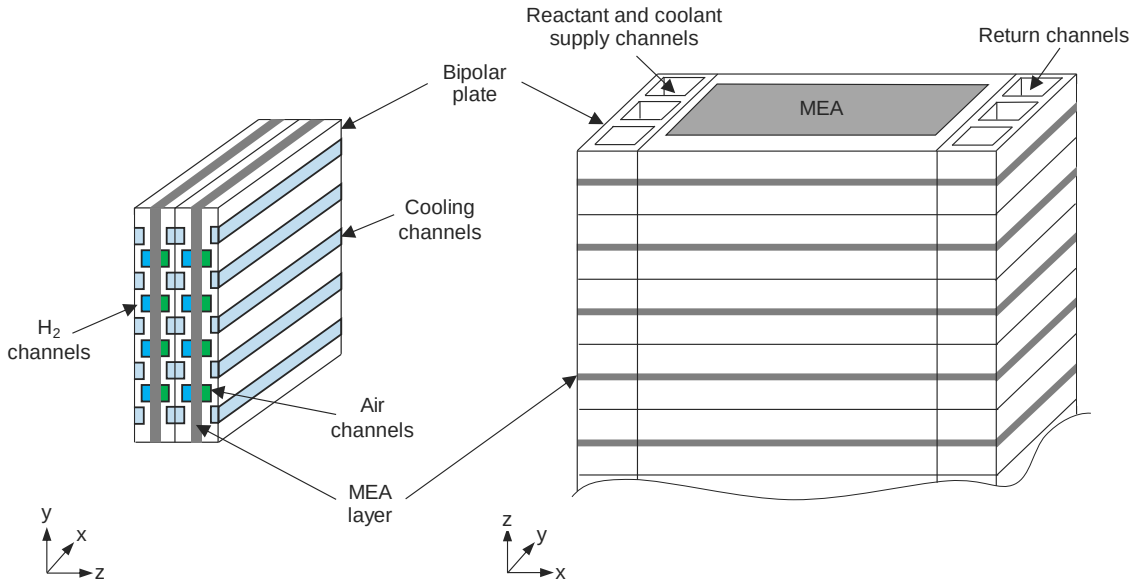

Figure 5: Schematic cut-section of two fuel cells connected with bipolar plates (left) and full stack (right) (not to scale)

Many flow field designs like parallel and serpentine channels have been investigated to achieve low pressure drops, large surface areas as well as a uniform temperature and reactant distribution over the cell, see e.g. [4], [5], [11] or [12] Due to non-uniform distribution of temperature and reactants over the cell and stack, the individual cell voltage and current varies. Pressure losses affect both coolant and reactants and the consumption of reactants reduces the hydrogen and oxygen concentration along the channels and cells further. These effects influence the local current density, temperature, humidity and thus performance of each cell. The specific distribution in a stack or cell also depends on the flow field design and arrangement of e.g. parallel, counter or cross flow of reactants and coolant. Some of these effects can be counteracted by higher coolant flow rates or reactant supply pressures but at the cost of increased parasitic power losses [4], [5], [10], [11], [12], [18], [19]. As a result, typical stack performance reduces by 5-20% compared to a single-cell [4] and increasing the size of the MEA often does not scale the current output accordingly [12].

2.1.3 Balance of plant

In order to supply the necessary reactants, regulate the FC pressure and maintain the operating temperature, additional auxiliary components are required. These components are summarized as the balance of plant (BoP) and can make up a large share of the total volume, weight and cost of the fuel cell system (FCS). Furthermore, the parasitic power loss of these components can reduce the efficiency of the FCS to a net efficiency of around 45% at rated power [3], [4], [6], [9]. For typical high-power FCS, the inlet air is supplied and pressurized by a compressor and a humidifier is required at one or both reactant inlets to ensure sufficient humidification of the membrane [4], [12]. Since both the air and hydrogen side are typically operated at stoichiometries higher than one, the waste of fuel needs to be minimized. Therefore, a recirculation loop is often installed on the anode side that also reduces the water loss and improves the membrane humidity. Due to the diffusion of inert gases like nitrogen from the cathode to the anode side, periodic purging is required to prevent the accumulation of nitrogen [11-12]. To integrate the FCS, for example into a vehicle, power electronics are required for power regulation and inversion. Furthermore, a cooling system for the thermal management of the FCS is required to maintain its operating temperature and preheat or cool the inlet gas streams [4], [12].

Thus, the design and operating conditions of PEMFC depend on many interdependent parameters that must be balanced together. Not only the impact of pressure and temperature on the Nernst potential, reaction kinetics and ohmic losses need to be considered but also, for example, spatial distributions, material choice, degradation effects and auxiliary devices to provide the desired operating conditions [4], [11], [12].

A detailed description of a FC with BoP and thermal management system integrated into a heavy-duty vehicle model is given in Paper II. More details on the BoP components can be found e.g. in [4], [6] and [12]. In the next section, an overview of the relevant heat transfer modes is presented.

2.2 Heat transfer

In this project, various forms of heat exchange occur, for example, (1) internal heat transfer in the FC, (2) heat rejection from the FC and other components to a coolant, (3) cooling or preheating of the reactant gases, (4) heat rejection from the coolant to the ambient air in a radiator and (5) heat transfer from the coolant to a water circuit and evaporative heat rejection in a novel bubble column cooling system, described in Paper I and III. The involved heat transfer modes are conduction, convection, radiation and phase change which can often occur simultaneously. In the following sections, an overview of heat transfer modes and heat exchangers is presented.

2.2.1 Conduction

Conduction describes the molecular heat transfer mode within solids and fluids without a moving fluid. Energy is transferred from molecules with higher temperature and thus kinetic energy to molecules with lower energy through collisions and in the case of metals also through free electrons [20-21]. An example of a steady-state conductive heat transfer through a series of one-dimensional solid walls without internal heat generation is shown in the following Figure 6:

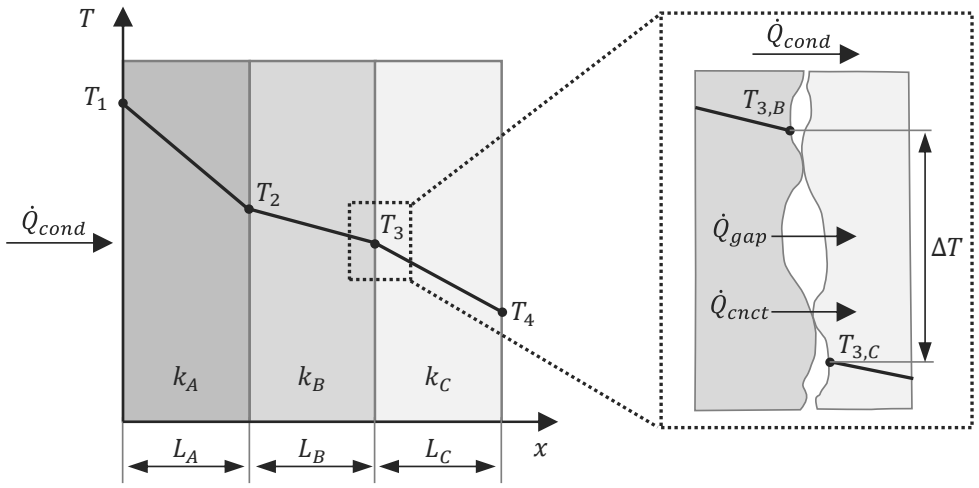

Figure 6: Schematic heat conduction through a series of solid walls with contact resistance, adapted from [21]

In the case of a single layer wall (A, ignoring wall B and C) the conductive heat transfer rate ($\dot{Q}_{cond}$) is described by a temperature gradient in the x-direction with length L_A and heat flowing from the higher

to lower temperature ($T_1 > T_2$). Conductive heat transfer is described by Fourier's law which results in a linear temperature change for a single layer with constant isotropic material properties as [21]:

$$\dot{Q}_{cond} = k_A \cdot A_w \cdot \frac{T_1 - T_2}{L_A} \tag{10}$$

with the thermal conductivity of the material (k_A) and wall area (A_w) through which the heat is conducted. Thermal conductivities are typically lowest for gases, followed by liquids and highest for solids, for example, 0.0246 W/mK for air, 0.6 W/mK for liquid water and 395 W/mK for copper [20].

When investigating several layers in series, the maximum conductive heat flow $\dot{Q}_{cond}$ is limited by the highest thermal resistance. The transferred heat through each layer is determined as [20-21]:

$$\dot{Q}_{cond} = \frac{A_w \cdot (T_1 - T_4)}{\frac{L_A}{k_A} + \frac{L_B}{k_B} + \frac{L_C}{k_C}} \tag{11}$$

Imperfect contact between solid body surfaces leads to an additional thermal contact resistance that reduces the transferable heat. The actual contact area is only around 1-2% of the total surface area, the remainder being fluid filled gaps. Which heat transfer modes are occurring in these microscopic gaps and how much heat is transferred through the contact spots ($\dot{Q}_{cnct}$) and the gaps ($\dot{Q}_{gap}$), respectively, depends on the solid material, type of fluid, temperature and size of the gaps. Higher contact pressures, reduced surface roughness or a gap fluid with high conductivity can reduce the contact resistance. The overall thermal resistance in the contact region causes an apparent temperature drop ΔT between the interface temperatures $T_{3,B}$ and $T_{3,C}$ [21-22].

In a FCS, heat is conducted, for example, through the solid parts of the MEA, to the BPP and potentially to the stack casing, adjacent components and the mountings. The actual contact area between the layers depends among others on the porosity and the clamping pressure [11]. In a heat exchanger, heat is, for example, conducted through the wall that separates the different fluids (see section 2.2.5). For more details on conduction and contact resistance, the reader is referred to e.g. [20-22].

2.2.2 Convection

Convection describes the combined heat transfer from conduction within a fluid and the energy transport due to the fluid flow. The heat transfer between a surface and a fluid not only depends on the temperature difference but also on the fluid velocity and the development of the boundary layers [20-21]. Further details on velocity, thermal and concentration boundary layers can be found e.g. in [21]. Figure 7 shows an exemplary external fluid flow over a plane wall with convective heat transfer from the fluid to and conductive heat transfer through the wall with a fully developed thermal boundary layer:

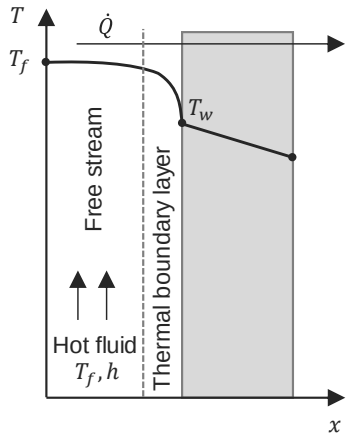

Figure 7: Schematic convection to and conduction through plane wall with fully developed thermal boundary layer (not to scale), adapted from [21]

Where T_f is the hot fluid temperature, h the convective heat transfer coefficient and T_w the wall temperature. The convective heat flow ($\dot{Q}_{conv}$) can be determined as:

$$\dot{Q}_{conv} = h \cdot A \cdot (T_w - T_f) \tag{12}$$

with the heat exchange area A. The heat transfer coefficient represents the complex flow conditions that influence the heat transfer besides the temperature difference. Depending on the cause of the fluid flow, two different types of convection are considered, forced and free convection. While the flow in forced convection is caused externally, e.g. by a pump or fan, the flow in free convection is caused by density difference due to temperature, pressure or concentrations gradients. Additionally, the flow regime of the fluid can either be laminar, transitional or turbulent, depending on geometry as well as fluid properties and velocity. The flow regime influences the fluid friction as wells as heat and mass transfer processes and is described by the Reynolds number (Re). For more details on laminar and turbulent flow, see e.g. [21]. To describe the typically experimentally determined heat transfer coefficients, similarity methods are used. Dimensionless numbers describe the empirical heat transfer and flow conditions for geometrically similar bodies with different fluids. The dimensionless Reynolds number not only describes the flow regime but also the characteristics of forced convection [20-21]:

$$Re = \frac{\rho \cdot v \cdot L}{\mu} \tag{13}$$

with the fluid density ρ, bulk fluid velocity v, dynamic viscosity μ and characteristic length L defined by the investigated system. For the description of the characteristics in free convection, the dimensionless Grashof number (Gr) is decisive:

$$Gr = \frac{L^3 \cdot g \cdot \beta \cdot (T_W - T_f)}{(\mu/\rho)^2} \tag{14}$$

with the gravitational acceleration $g = 9.81$ m/s² and thermal volume expansion coefficient β. Additional fluid properties that are relevant for both forms of convection are represented by the dimensionless Prandtl number (Pr):

$$Pr = \frac{c_p \cdot \mu}{k} \tag{15}$$

with the specific heat capacity of the fluid c_p and thermal conductivity k. The dimensionless heat transfer coefficient is expressed as the Nusselt number (Nu), from which the convective heat transfer coefficient (h) can be determined:

$$Nu = \frac{h \cdot L}{k} \tag{16}$$

This results in the description of the dimensionless heat transfer coefficient for forced convection in general terms as:

$$Nu_{forced} = f(Re, \mathrm{Pr}) \tag{17}$$

and for free convection as:

$$Nu_{free} = f(Gr, \mathrm{Pr}) \tag{18}$$

Typical heat transfer coefficient values for free convection are 2-25 W/m²K in gases and 10-1,000 W/m²K in liquids. Significantly higher values can be reached with forced convection typically ranging from 25-250 W/m²K in gases and 50-20,000 W/m²K in liquids [20-21].

In a FC, convective heat transfer occurs, for example, in the cooling and gas channels, the porous electrodes and at the surface of the stack. In heat exchangers, for example, in the respective fluid flow channels to exchange heat through a solid wall (see section 2.2.5). For more details convective heart transfer, the reader is referred to e.g. [20-21].

2.2.3 Phase change

A special case of convection is the phase change associated with evaporation, boiling and condensation. In addition to the sensible heat exchange due to the involved fluid motion, also latent heat is exchanged when changing between a liquid and vapor. This requires heat input for evaporation or boiling and releases heat during condensation [20-21]. Additionally, latent heat can be utilized in phase change materials (PCM) that change between a solid and liquid state. Further details on thermal management with refrigerants, water evaporation and PCMs follow in section 2.3.

The most relevant phase change process for this project is the evaporation of water into air, i.e. the phase change from liquid to vapor below the boiling temperature of water. Evaporative convection processes additionally include the transfer of mass from one fluid to another based on concentration differences, e.g. when unsaturated air is flowing over a water surface, vapor is transferred to the air. This process therefore also involves a concentration boundary layer and mass diffusion processes that can be described analogously to the temperature driven convection processes, see e.g. [21]. During this phase change, the latent heat of vaporization is required to enable the liquid molecules to overcome the surface binding energy and must either be provided by the liquid itself, the gas into which the vapor is evaporated or an external heat source [20-21]. The latent heat ($\dot{Q}_{lat}$) that is required to evaporate a certain amount of liquid ($\dot{m}_{evap}$) is defined as:

$$\dot{Q}_{lat} = \dot{m}_{evap} \cdot \Delta h_v \tag{19}$$

with the temperature and fluid dependent heat of vaporization Δh_v. The water content in air can be defined as the humidity ratio (ω), the ratio of vapor (m_v) to dry air mass ($m_{a,dry}$) [11], [12], [20], [23]:

$$\omega = \frac{m_v}{m_{a,dry}} \tag{20}$$

Alternatively, it can be expressed as the relative humidity (φ), defined as the ratio of the partial vapor pressure (p_v) and vapor saturation pressure ($p_{v,sat}$):

$$\varphi = \frac{p_v}{p_{v,sat}} \;\; with \;\; 0 \leq \varphi \leq 1 \tag{21}$$

The vapor saturation pressure is a function of temperature only and describes the maximum amount of water vapor that the air can hold at the given conditions. Both parameters are coupled by the following equation:

$$\omega = \frac{M_w}{M_a} \cdot \frac{\varphi \cdot p_{v,sat}}{p - \varphi \cdot p_{v,sat}} \tag{22}$$

with a ratio of molar mass of water M_w to air M_a of around 0.622 and the total pressure p. The following Figure 8 shows the amount of water that air can hold (humidity ratio) as a function of the temperature and relative humidity at 1 atm based on equation (22):

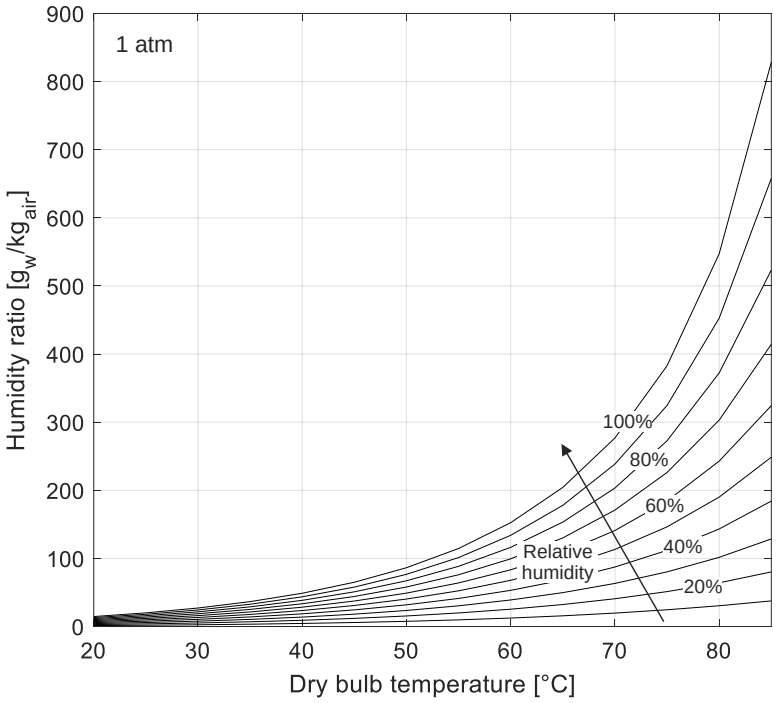

Figure 8: Humidity ratio as a function of temperature and relative humidity at 1 atm

Since the amount of water that the air can hold increases exponentially with temperature, high operating temperatures of the FC increase the drying effect of the air flow on the membrane. As further described in e.g. [11-12], these correlations allow to determine water evaporation rates and heat uptake/release for the relevant processes in a FC, e.g. in the porous electrodes. Furthermore, they are relevant for designing and modelling of the bubble evaporation cooling system described in Paper I and III. More details on phase change and the process of air humification can be found e.g. in [11], [12], [20] and [21].

2.2.4 Radiation

Thermal radiation is the energy emitted from a body in the form of electromagnetic waves which do not require a transport medium [20-21]. A radiative (and convective) heat transfer example of a semitransparent plate with surface temperature T_s is shown in the following Figure 9:

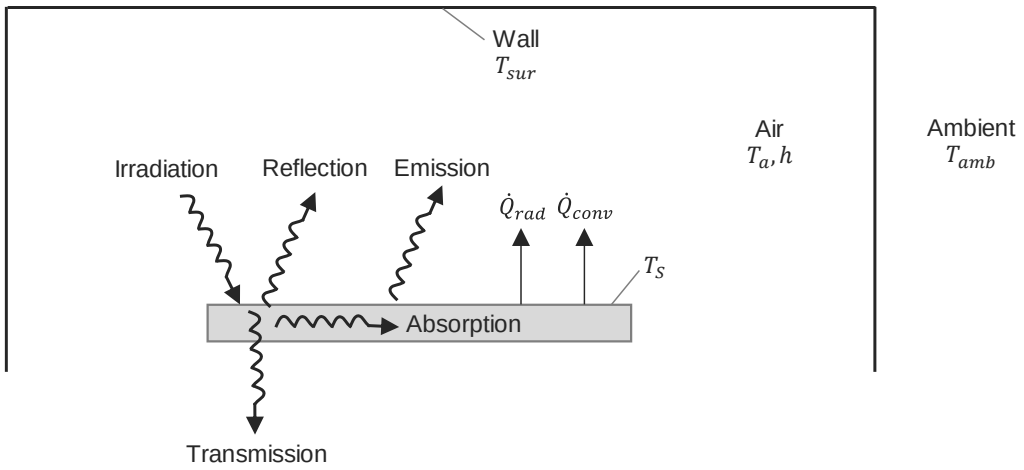

Figure 9: Schematic radiative and convective heat transfer from a semitransparent plate into a large surrounding with $T_s > T_{sur}$, $T_s > T_a$ (not to scale), adapted from [21]

The surface area of the surrounding environment, e.g. the wall of a room, is assumed to be large compared to the plate surface area (A). The surrounding temperature (T_{sur}) is not necessarily equal to the air temperature that directly surrounds the plate (T_a), for example due to the impact of the ambient temperature (T_{amb}) on the wall. Due to $T_s > T_{sur}$ and $T_s > T_a$, heat is transferred by radiation ($\dot{Q}_{rad}$) and convection from the plate. The radiative heat transfer can be determined as [20-21]:

$$\dot{Q}_{rad} = \varepsilon \cdot \sigma \cdot A \cdot (T_s^4 - T_{sur}^4) \;\; with \;\; 0 \leq \varepsilon \leq 1 \tag{23}$$

with the Stefan-Boltzmann constant $\sigma = 5.67 \cdot 10^{-8}$ W/(m²K⁴) and the emissivity ε. Real surfaces emit radiation depending on their temperature, the radiation wavelength, direction of radiation as well as surface structure and material, described by the emissivity. The assumption of constant emissivity with $\varepsilon < 1$ leads to a so-called gray body as a representation of real bodies compared to the hypothetical black body which emits the maximum possible radiation only depending on its temperature ($\varepsilon = 1$). The assumption of a gray body is accurate for many surfaces [20-21] and emissivity values are tabulated for typical materials and surface finishes, e.g. in [20].

In addition to emitting radiation, surfaces can also absorb, transmit or reflect incoming radiation (irradiation) from other bodies. While black bodies absorb all incoming radiation, the absorptivity of gray bodies is equal to their emissivity and the remaining incoming radiation is either transmitted, reflected or both, depending on the material. Bodies that face each other exchange radiative heat depending on the orientation of the surfaces. View factors can be determined to describe how radiation is exchanged between surfaces [20-21].

In FCs and heat exchangers, radiation transfers heat within the gas channels and from the outer surface to the surrounding. For more details on electromagnetic radiation and radiative heat exchange of real bodies, the reader is referred to e.g. [20-21].

2.2.5 Heat exchanger

The device used to transfer heat from one fluid to another is called heat exchanger and many different types have been developed for a variety of applications [21]. Figure 10 schematically shows a parallel flow heat exchanger section in which heat is convectively transferred from the hot fluid channel to the wall, then conductively through the wall and eventually convectively from the wall to the cold fluid:

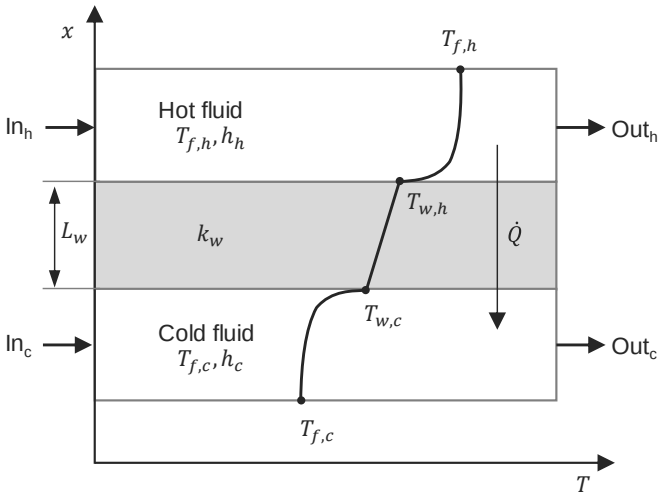

Figure 10: Schematic heat transfer from a hot to cold fluid channel through the separating wall in a parallel flow heat exchanger section (not to scale), adapted from [21]

with the hot and cold fluid temperature $T_{f,h/c}$, hot and cold side convective heat transfer $h_{h/c}$, the hot and cold side wall temperature $T_{w,h/c}$ as well as wall conductivity k_w and thickness L_w. Alternative to the parallel flow, the flows could be oriented in opposite (counterflow) or perpendicular direction to each other (crossflow) which affects the achievable heat transfer. The number of passages describes how often the fluids pass through the heat exchanger to exchange heat. Fins are often used in gas flow channels to increase the surface area due to the lower convective heat transfer coefficients compared to liquids [21].

Depending on the given parameters, different approaches can be used to design a heat exchanger. If the desired/required inlet and outlet temperatures are known, the log mean temperature difference method can be used. In systems like a heat exchanger which involve several modes of heat transfer (compare Figure 10), the transferable heat can be described by an overall heat transfer coefficient (U) [20-21]:

$$\dot{Q} = U \cdot A \cdot \Delta T_{lm} \tag{24}$$

with the logarithmic mean temperature ΔT_{lm} and overall heat exchanger area A. When neglecting fins, fouling effects and radiation, the overall heat transfer coefficient can be derived from the series connection of thermal resistances caused by convection and conduction:

$$\frac{1}{U \cdot A} = \frac{1}{h_h \cdot A_h} + \frac{L_w}{k_w \cdot A_w} + \frac{1}{h_c \cdot A_c} \tag{25}$$

with the heat exchange area on the hot and cold side $A_{h/c}$ and mean conductive heat transfer area of the wall A_w. The local temperature difference between the hot and cold fluid depends on the position in the heat exchanger. A logarithmic mean temperature captures these effects along the heat exchanger and is expressed as:

$$\Delta T_{lm} = \frac{\Delta T_1 - \Delta T_2}{\ln\left(\frac{\Delta T_1}{\Delta T_2}\right)} \tag{26}$$

with the temperature difference at inlet ΔT_1 and outlet ΔT_2, adjusted to the parallel- or counterflow arrangement, respectively.

Additionally, the transferred (sensible) heat ($\dot{Q}$) can be derived from an energy balance without phase change and neglectable heat losses to the surroundings of the heat exchanger, resulting in [21]:

$$\dot{Q} = \dot{m}_h \cdot c_{p,h} \cdot (T_{h,i} - T_{h,o}) = \dot{m}_c \cdot c_{p,c} \cdot (T_{c,i} - T_{c,o}) \tag{27}$$

with the hot and cold mass flow rate $\dot{m}_{h/c}$, mean fluid temperatures on hot and cold inlet and outlet side $T_{h/c,i/o}$ and the specific heat of the hot and cold fluid $c_{p,h/c}$.

If only the inlet temperatures are known, the effectiveness NTU method is the preferable method to determine the heat exchange rate and thus outlet temperatures. The effectiveness of a heat exchanger (ε) is defined as the ratio of transferred heat ($\dot{Q}$) to maximum theoretically transferable heat ($\dot{Q}_{max}$) [21]:

$$\varepsilon = \frac{\dot{Q}}{\dot{Q}_{max}} \quad with \;\; 0 \leq \varepsilon \leq 1 \tag{28}$$

The maximum theoretically transferable heat is limited by the highest temperature difference in the heat exchanger, i.e. the hot inlet minus the cold inlet temperature, and the lower of the heat capacities of both fluids:

$$\dot{Q}_{max} = C_{min} \cdot (T_{h,i} - T_{c,i}) \tag{29}$$

with the minimum (C_{min}) and maximum heat capacity (C_{max}) either being $C_h = \dot{m}_h \cdot c_{p,h}$ or $C_c = \dot{m}_c \cdot c_{p,c}$, depending on which is lower or higher, respectively. The dimensionless number of transfer units (NTU) is defined as:

$$NTU = \frac{U \cdot A}{C_{min}} \tag{30}$$

and empirical and graphical correlations have been determined for many heat exchangers that allow the determination of the heat exchanger effectiveness based on $\varepsilon = f(NTU, C_{min}/C_{max})$, see e.g. [20-21]. Thus, the transferred heat can be determined from the heat exchanger effectiveness as:

$$\dot{Q} = \varepsilon \cdot C_{min} \cdot (T_{h,i} - T_{c,i}) \tag{31}$$

For more details on the design, different types and modelling of heat exchangers, the reader is referred to e.g. [20-21].

2.3 Fuel cell thermal management

The (local) FC temperature directly influences its performance and lifetime, i.e. higher temperatures are beneficial for the reaction kinetics but accelerate degradation and dry out the membrane due to increased evaporation rates while lower operating temperatures slow down kinetics and favor condensation and thus the risk of flooding. This results in an optimum operating temperature range of 60-80°C with temperatures up to 90°C for short periods, depending on the operating conditions and system level cooling requirements. This low operating temperature leads to difficulties in achieving sufficient heat rejection to maintain target operating temperature on the FC and cooling system side. In the FC itself,

the low operating temperatures lead to negligible heat rejection by the exhaust gases and therefore, the cooling system needs to reject the majority of the heat [3], [4], [5], [9], [10], [11]. Liquid cooled FCS typically reject heat to ambient with a radiator where the low temperature difference to the surrounding air leads to significantly increased radiator sizes of 1.5 – 4 times larger frontal areas compared to internal combustion engines, depending on the application and operating profile. This complicates packaging and can increase the drag of the vehicle [5], [9], [18], [24], [25].

The degradation of the FC decreases the available voltage and power at the end of life (EoL), typically defined by a voltage reduction of 10% [8]. The heat load at the EoL therefore increases (compare e.g. [26]) and compensating for the power loss by correcting the operating point to higher current densities can elevate it further [27]. Additionally, thermal management systems directly impact the cost, performance and durability of FCS and can make up a large share of the parasitic power losses [5], [24], [28].

Depending on the application and thus desired power output of the FC, different cooling solutions are required. Below 100 W, passive cooling is sufficient but for higher power active cooling is required. Low power applications, typically below 1-2 kW, can be sufficiently cooled with active air cooling. At higher power levels, liquid cooling becomes necessary which utilizes the higher heat capacity and heat transfer coefficients of liquids compared to gases, typically by running the coolant through the bipolar plates. Deionized water combined with an antifreeze like ethylene-glycol is often used as a coolant [4], [5], [12].

Alternative solutions have been developed to complement, replace or modify the liquid cooling loop. Most investigations that address the thermal management of high-power PEMFCs focus on passenger cars with lower power requirements and thus heat loads compared to HD vehicles. These alternatives include the use of phase change to either increase the heat removal from the FC itself, from the vehicle to the ambient or to store heat temporarily. Evaporation of water can, for example, be used by direct injection into the FC or reactant inlet stream to cool the cell and simultaneously support membrane humidification [5], [16], [29], [30]. Evaporation of water can also be used to increase the heat rejection to ambient by, for example, spraying water on the radiator [18], [31], investigated also for HD heat loads [26], [32]. To remove heat from the cell by boiling in the cooling channels, typically refrigerants are required at standard operating pressures due to the low temperature of PEMFCs [5], [16], [33], [34]. Besides boiling in the FC cooling channels, the integration of the FC cooling system with the air conditioning refrigeration cycle has been investigated [5], [35], [36]. Temporarily storing heat at peak power production and releasing it later can be achieved by melting and solidifying PCMs with low melting temperatures and high latent heat like a paraffin wax [37-38].

Waste heat recovery has been investigated as an alternative to rejecting the heat from the vehicle but requires that heat, electrical or mechanical power can either be used or stored in the system. Heat can be integrated to e.g. preheat the reactants or release stored hydrogen from metal hydride tanks. Heat to power could be achieved e.g. by organic Rankine cycles or the use of thermoelectric generators, although typically resulting in low efficiencies due to the low grade heat (<100°C) [6], [39]. Extensive reviews of cooling methods, including alternatives to remove the heat from the cell, alternative cooling fluids and waste heat recovery methods, are presented in e.g. [5], [18], [29], [34] and [39].

Alternative cooling solutions to overcome the thermal limitations of high-power PEMFCs in HD vehicles by complementing or replacing the conventional cooling should ideally be of low complexity, cost, additional weight/volume and power consumption as well as use fluids that are not harmful, non-flammable, are compatible with the FC materials and have low global warming potentials [5], [18], [39].

Within this project, the thermal management focus is on worst case cooling to prevent overheating of the FC and thus to avoid vehicle performance loss from FC power derating, accelerated degradation and damage of the FC. Start-up behavior and low temperature challenges like freezing are not further investigated, details can be found e.g. in [3], [6] and [11].

2.4 Longitudinal vehicle dynamics

The necessary traction power that the propulsion system has to provide is determined from the traction force (F_{trac}) that must overcome the driving resistances acting on a vehicle. In a simplified model, these consist of three major forces: (1) the road slope (F_{slope}), (2) vehicle drag (F_{drag}) and (3) rolling resistance (F_{roll}). Additionally, the acceleration (dv/dt) of the vehicle and the inertia of rotating parts, included in the total vehicle mass ($m_{veh,t}$), must be considered [40-41]:

$$F_{trac} = F_{slope} + F_{roll} + F_{drag} + m_{veh,t} \cdot \frac{dv}{dt} \tag{32}$$

These forces are schematically shown for an uphill drive in the following Figure 11:

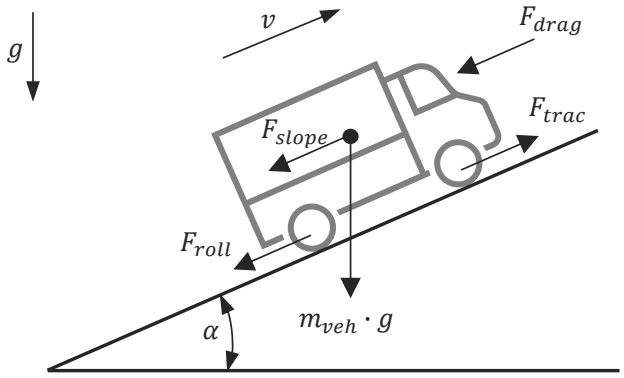

Figure 11: Schematic driving forces acting on a vehicle driving uphill, adapted from [40]

If the vehicle is driving uphill, i.e. non-horizontally, a force is caused by gravity ($g = 9.81$ m/s²) which depends on the slope α:

$$F_{slope} = m_{veh} \cdot g \cdot \sin(\alpha) \tag{33}$$

Since the friction losses of the tires depend on the force with which they are pressed to the road surface, they are also influenced by the slope:

$$F_{roll} = m_{veh} \cdot g \cdot f_r \cdot \cos(\alpha) \tag{34}$$

A rolling friction coefficient f_r represents the different influences on the rolling resistance like the tire pressure, vehicle velocity or surface conditions like wheel slip, a dry or wet surface and driving on concrete, sand or other surfaces.

The viscous friction, difference in pressure between the front to rear of the vehicle and resistance from flow through the car body, e.g. from radiators, cause an aerodynamic drag on the vehicle. This drag can be expressed by a drag coefficient c_d:

$$F_{drag} = \frac{1}{2} \cdot \rho_{air} \cdot c_d \cdot A_{front} \cdot v^2 \tag{35}$$

with the air density ρ_{air}, frontal area of the vehicle A_{front} and neglected front and side winds.

Finally, the inertia of the rotating parts, i.e. powertrain and wheels, can be summarized as an effective rotating mass (m_r) which is added to the vehicle mass (m_{veh}), neglecting losses in the transmission and assuming no wheel slip:

$$m_{veh,t} = m_{veh} + m_r = m_v + \frac{1}{r_w^2}\Theta_{\mathrm{w}} + \frac{\gamma^2}{r_w^2}\Theta_p \tag{36}$$

with the wheel radius r_w, gear ratio γ as well as total wheel Θ_{w} and powertrain moment of inertia Θ_p. Further details of longitudinal vehicle dynamics can be found e.g. in [40-41]. In the next chapter, a summary of the publications from this project thus far is presented.

Chapter 3

Summary of publications

In the following chapter the published and submitted work is summarized in a project-chronological order. A first approach to improve the heat rejection capabilities of FCEV was made by investigating the viability of an ammonia sorption heat transformer (Conference Presentation I). To investigate the thermal limitations of PEMFC on a vehicle level, a modular high-power FC stack with BoP model has been developed, resulting in the verified HD FC truck vehicle model. The thermal limitations of conventional cooling systems identified in this truck model (Paper II) enabled the development of an alternative solution to complement the conventional cooling system with a bubble column evaporator cooling system (Paper I). A proof-of-concept test bench was built to verify the viability of the concept (Paper III).

3.1 Ammonia absorption heat transformer (Conference Presentation I)

Ammonia sorption heat pump for PEM fuel cell thermal management in heavy duty transport
Presented at the 8th Thermal and Fluids Engineering Conference (TFEC)
Presentation only
Christian Boßer, David Sedarsky
2023

In a brief first attempt to address the heat rejection limitations of PEMFCs, an ammonia (NH_3) absorption heat transformer (AHT) was investigated, presented in Conference Presentation I. The main concept is to increase the coolant temperature and thus the temperature difference to the ambient air to improve the heat rejection capabilities of the FC cooling system with an AHT. A heat transformer is a special form of heat pump which is driven by a heat input, in this case the FC waste heat, which is converted into heat at a higher temperature. AHTs have previously been combined with a 5 kW PEMFC by A. Huicochea et al. for water purification with H_2O-LiBr as working fluids, the most common type of AHT [42-43]. The process is driven by the exergy provided by the waste heat, requiring electricity of less than 1% of the thermal energy input and providing an inherent heat storage capacity [44-45]. Ammonia as a refrigerant has the advantage of no global warming potential, high latent heat at a low boiling point and it is chemically stable and of low corrosivity [46-47]. But practical issues of ammonia sorption heat transformers like its typically large industrial size, high weight and cost, high operating pressure, toxicity and flammability of ammonia, low maturity level and the low coefficient of performance of heat transformers led to the conclusion that it is not a viable solution for transport applications [44], [46], [47], [48], [49].

The process is realized by an evaporation-absorption-generation-condensation process, depicted in the following Figure 12:

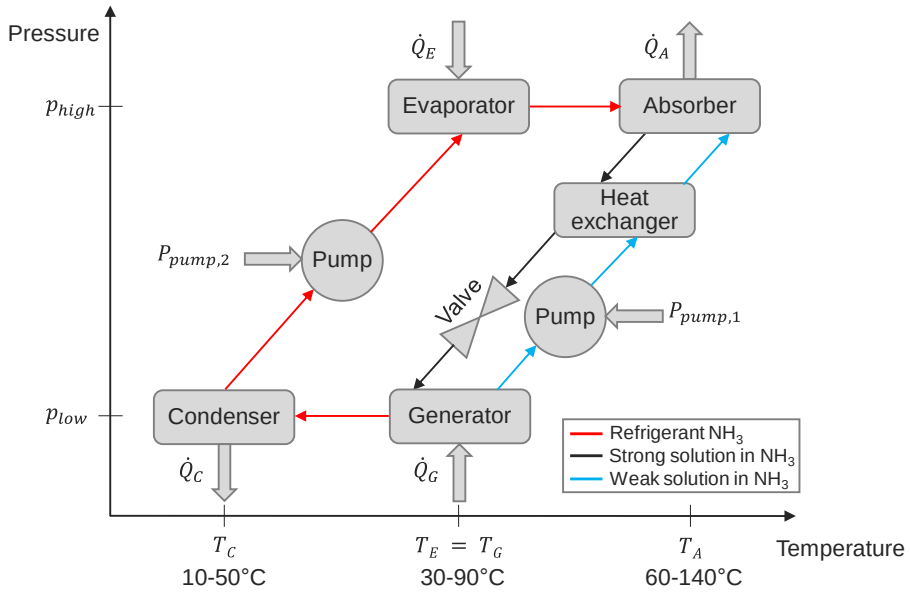

Figure 12: Working principle sorption heat transformer with NH_3 operating temperature range, adapted from [44], [48], [50]

Due to the heat input at an intermediate temperature T_E, ammonia is evaporated in the evaporator. The vapor then gets absorbed into e.g. H_2O or $LiNO_3$ in the absorber, a process that releases heat at a higher temperature T_A. This results in a solution that is strong in NH_3 which gets throttled through a valve in the generator. Intermediate temperature input in the generator desorbs NH_3 vapor from the solution again and the weak solution is pumped back to the absorber, exchanging heat with the strong solution. The ammonia vapor on the other hand is condensed in the condenser and pumped back to the evaporator. The shown temperature ranges represent the operating range for ammonia based AHTs which require $T_A > T_E = T_G > T_C$. With higher desired temperature lift, the effectiveness and required condensation temperature decrease [44], [48], [50].

Its effectiveness is defined by the coefficient of performance, the ratio of heat that can be upgraded to higher temperatures ($\dot{Q}_A$) to the total input heat ($\dot{Q}_E + \dot{Q}_G$) and pump power ($\sum P_{pumps}$) required to drive the process [48]:

$$COP = \frac{\dot{Q}_A}{\dot{Q}_E + \dot{Q}_G + \sum P_{pumps}} \tag{37}$$

The practical upper limit for the COP for ammonia AHTs is around 0.5 [46], [48], [50], decreasing e.g. with increasing condensation temperatures [44], [46] which is problematic in automotive radiators at high ambient temperatures. This results in the biggest disadvantage of the concept since more than half of the FC waste heat needs to be rejected in the condenser at temperatures even lower than the FC operating temperature, diminishing the gains of the improved heat rejection at higher temperatures. Further details can be found e.g. in [43], [44], [49] and [50].

A simplified investigation of a single stage AHT with a constant COP of 0.5 and neglected heat storage capacity and heat transfer process into the AHT was conducted with a validated 5 kW FC model developed in Siemens Simcenter Amesim. It confirmed the disadvantage of rejecting half of the FC at lower temperatures from the condenser despite the benefits of the elevated temperature for the other half

of the heat. Additionally, the complexity of the cooling system increased significantly due to the two additional cooling systems (high and low temperature) as well as the sorption heat transformer itself.

3.2 PEMFC truck vehicle model with conventional cooling system (Paper II)

Verified PEM fuel cell heavy-duty long-haul truck vehicle model with thermal management limitations of conventional cooling systems
Submitted manuscript
Christian Boßer, David Sedarsky
2025

In Paper II, we present the development, verification and thermal limitations of a 0D/1D modular HD truck vehicle model with conventional cooling system in Siemens Simcenter Amesim at beginning of life conditions. It provides a platform that cannot only be used for future investigations of thermal management, degradation effects and enhanced FC modelling within the research group but also provides a modelling approach for other projects to investigate e.g. advanced energy management strategies or component sizing studies. Investigating PEMFC systems and thermal management from a holistic perspective in a comprehensive vehicle model enables the investigations of the interdependencies between the large amount of involved components, FC operation and ambient conditions. Furthermore, the modular structure allows the adaptation to other modes of HD transport like planes, ships or trains.

The main components of the modelled powertrain are two FCS, a Li-ion battery, two electric traction machines and three dedicated cooling loops. A conceptual integration of the three radiator-fan-assemblies into the 44 t EU truck is shown in the following Figure 13:

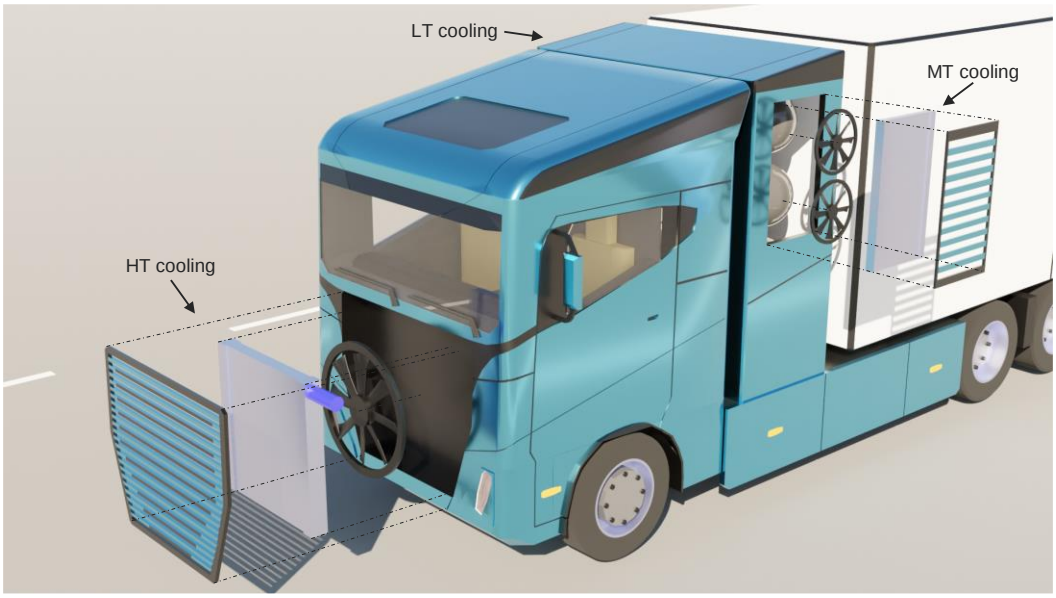

Figure 13: Conceptual vehicle integration of the HT, MT and LT radiators

The high temperature (HT) cooling loop is positioned unobstructed in the front of the vehicle, maximizing the available space and heat rejection capabilities in an existing truck platform, not requiring a structural redesign of the cab. To capture the additional heat rejection requirements and power

consumptions of the medium (MT) and low temperature (LT) cooling loops, the radiators are positioned in the side panels behind the driver. Severe thermal limitations of the FC have been found in hill climbs already at 20°C and due to the integration of braking resistors to substitute engine braking also during downhill driving. Accurate identification of these limitations of conventional cooling systems in FCEVs enables the development of improved thermal management solutions that can either replace or, as presented in the following Paper I and III, complement these established radiators in existing truck platforms.

3.3 Continuous bubble column evaporator cooling concept (Paper I)

Bubble column evaporative cooling for PEMFC thermal management in heavy-duty vehicles
Presented at the 10th Thermal and Fluids Engineering Conference (TFEC), Begel House Inc.
doi: 10.1615/TFEC2025.mes.055991
Christian Boßer, David Sedarsky
2025

Based on the identified thermal limitations of the conventional radiator, presented in Paper II, a highly integrated, complementary evaporative cooling solution has been developed. The system has been dimensioned for steady-state full FC load at a highway speed of 85 km/h.

Additional heat rejection and thus cooling of the FC is achieved by utilizing the high latent heat of the FC product water. Various methods of evaporating water at sub-boiling point conditions exist, for example, by spraying the water on the HT radiator. Alternatively, literature shows high heat and mass transfer for evaporation of the water in a bubble column. Figure 14 shows the concept of integrating this evaporator into the FCS and HT cooling loop:

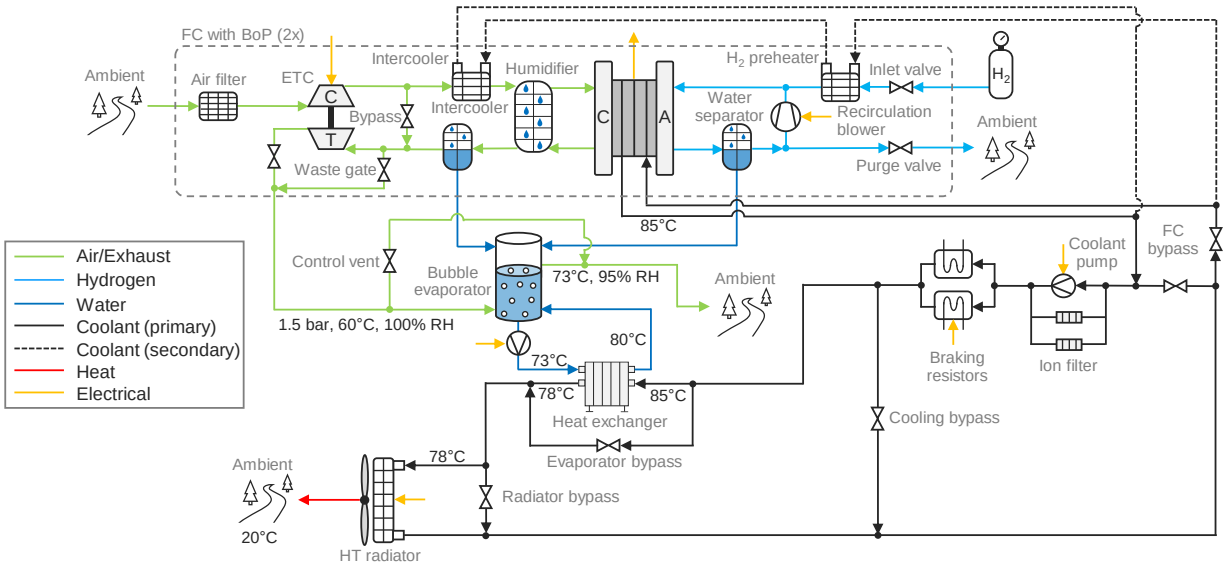

Figure 14: Bubble column evaporator integration into FCS and HT cooling loop

First, the heat is transferred from the FC coolant to an additional water circulation loop in a heat exchanger. The water circuit circulates the captured FC product water which is either evaporated by utilizing the FC exhaust air flow, effectively expanding the pressure recovery of the compressor work, or a separate blower. Thus, full FC load could be achieved at 20°C and 35°C and with additional but

feasible measures also at 45°C. Depending on the amount of stored water, the increased heat rejection can be achieved for 11-58 min with 20-100 kg water storage, respectively.

The system offers the advantage of, among others, working without additional radiator surface area and thus no drag increase, low additional input power, improving performance with altitude and only utilizing safe fluids, i.e. FC product water and air. The developed concept is a FC specific solution due to the onboard water production but not only limited to HD trucks. Open questions remain regarding practical implementations like possible air flow ratios, compactness of the system, vehicle control strategy integration and G-forces, noise or freezing conditions.

3.4 Bubble column evaporator cooling redesign and proof-of-concept (Paper III)

Evaporative bubble column cooling for PEMFC heavy-duty vehicle thermal management with experimental proof-of-concept
Submitted manuscript
Christian Boßer, David Sedarsky
2025

In Paper III, we extend the investigations of Paper I by showing the setup and results of a proof-of-concept test bench to evaluate the viability of the theoretical bubble column evaporator cooling concept for PEMFC HD vehicles. The system has been redesigned to a counterflow layout based on the lessons learned from the experimental investigations, reducing the involved amount of water significantly and making the system more compact.

To represent the conditions of the vehicle size system accurately, the same air to water flow ration of around 46 has been kept in the small scale test bench. Air flow rates of 250-1600 L/min have been investigated in a bubble column with 0.2 m outer diameter. The resulting superficial gas velocities of up to 0.966 m/s, defined as the ratio of air volume flow rate to effective cross sectional column area, showed even higher heat rejection rates than predicted, potentially caused by higher evaporation temperatures than assumed. This suggests that even lower water levels or higher air flow rates might be possible than theoretically determined, potentially reducing the system size or the required FC operating temperature. Previously, the high evaporation effectiveness of bubble columns has only been reported for superficial gas velocities of up to 0.3 m/s.

Open questions remain regarding the upper heat rejection limits, exact causes for the increased heat rejection rates and if the system scales as expected when increased to full vehicle size. Additional investigations with measurement of air inlet and outlet conditions, temperature fields in the column, FCS outlet conditions, higher water temperatures and scaling to full size are required. A dynamic simulation model is required for validation and development of the vehicle integration and control.

Chapter 4

Concluding remarks

Summarizing, first the technical background of PEMFCs, heat transfer, FC thermal management and longitudinal vehicle dynamics have been presented, followed by a summary of the results from the "PEM fuel cell thermal management for high performance" project. Starting from a small scale 0D/1D FC model developed in Siemens Simcenter Amesim, a comprehensive, modular and verified truck vehicle model with a high power FCS has been developed. This baseline model has been used to identify the thermal limitations of conventional cooling systems in HD FCEV from which an alternative bubble column evaporator cooling system has been derived. Its viability was shown on a proof-of-concept test bench. In the following final section, an overview of the planned investigations within this project and how they connect to the overall collaborative goal of a holistic approach to FC modelling, thermal management and lifetime investigations for FCEV is presented.

4.1 Future work

Three major aspects are planned to be further investigated from a PEMFC thermal management perspective in HD applications: (1) FC thermal management on a vehicle level, (2) bubble column evaporative cooling and (3) enhanced FC simulation models.

In order to enhance the existing FC simulation models, a 1D MEA modelling approach is currently collaboratively under development within the research group. It allows for a spatial distribution of the different MEA layers and thus more detailed modelling of mass and heat transfer as well as water management, degradation and heat production. A modelling approach to form a multi-cell stack has been developed to investigate non-uniformities on a stack level. The single cell and short stack shall be validated against measurements on a custom FC test bench. A simulation model of this FC test bench has been built in Amesim, including an advanced cooling/heating system that allows to impose a temperature difference on the cathode and anode side of a single cell. With this temperature gradient, the overall heat transfer through a cell can be determined or different positions of a cell in a stack simulated. For the realization of this test bench, an exchange to the partner company Hydroxide Technologies is planned. The resulting FC model shall eventually be integrated into the modular structure of the developed FCS and vehicle model.

The next steps in the development of the bubble evaporative cooling system are to finalize and validate a dynamic model of the test bench system with the measurements and assumptions presented in Paper III. This dynamic model will then be scaled to full vehicle size, with the assumption that it scales accordingly. Missing components like the heat exchanger and FC product water capture will be added and the system integrated into the FC HT cooling loop and FC exhaust of the truck vehicle model. To

operate the system in the vehicle, a control strategy needs to be developed. Further measurements on a refined and full size test bench would be valuable to validate the observed behavior at scale.

Additional vehicle level investigations on the limits of conventional cooling systems in FCEV could include (1) the achievable gains with an ideal cooling system, (2) the impact of increased cooling fan speed and power on the net power gain of the FCS, (3) the impact of higher ambient temperatures or (4) increased battery sizes. Finally, full vehicle level investigations can be conducted that include the enhanced FC model and bubble evaporative cooling system. This allows for simultaneous investigations of the interdependency of the involved components, FC operation, degradation effects, parasitic power losses as well as water and thermal management over the lifetime of the vehicle in the different collaborative projects. Due to the modular FCS and vehicle structure as well as the vehicle type independent viability of the bubble column cooling system, the developed solutions shall be transferred to other modes of HD transport like planes.

References

[1] “CO2 emissions from cars: facts and figures (infographics),” European Parliament. Accessed: Apr. 29, 2025. [Online]. Available: https://www.europarl.europa.eu/topics/en/article/20190313STO31218/co2-emissions-from-cars-facts-and-figures-infographics

[2] “Emissions from planes and ships: facts and figures (infographic),” European Parliament. Accessed: May 08, 2025. [Online]. Available: https://www.europarl.europa.eu/topics/en/article/20191129STO67756/emissions-from-planes-and-ships-facts-and-figures-infographic

[3] D. A. Cullen *et al.*, “New roads and challenges for fuel cells in heavy-duty transportation,” *Nat. Energy*, vol. 6, no. 5, Art. no. 5, Mar. 2021, doi: 10.1038/s41560-021-00775-z.

[4] R. P. O’Hayre, S.-W. Cha, W. G. Colella, and F. B. Prinz, *Fuel cell fundamentals*, Third edition. Hoboken, New Jersey: John Wiley & Sons Inc, 2016.

[5] G. Zhang and S. G. Kandlikar, “A critical review of cooling techniques in proton exchange membrane fuel cell stacks,” *Int. J. Hydrog. Energy*, vol. 37, no. 3, Art. no. 3, Feb. 2012, doi: 10.1016/j.ijhydene.2011.11.010.

[6] S. Pardhi, S. Chakraborty, D.-D. Tran, M. El Baghdadi, S. Wilkins, and O. Hegazy, “A Review of Fuel Cell Powertrains for Long-Haul Heavy-Duty Vehicles: Technology, Hydrogen, Energy and Thermal Management Solutions,” *Energies*, vol. 15, no. 24, Art. no. 24, Jan. 2022, doi: 10.3390/en15249557.

[7] M. Pihlatie, M. Ranta, P. Rahkola, and R. Åman, “Zero-Emission Truck Powertrains for Regional and Long-Haul Missions,” *World Electr. Veh. J.*, vol. 14, no. 9, Art. no. 9, Sep. 2023, doi: 10.3390/wevj14090253.

[8] J. Marcinkoski, R. Vijayagopal, J. Adams, B. James, J. Kopasz, and R. Ahluwalia, “Hydrogen Class 8 Long Haul Truck Targets (US Department of Energy),” 2019, [Online]. Available: https://www.hydrogen.energy.gov/ pdfs/19006_hydrogen_class8_long_haul_truck_targets.pdf

[9] K. Mayr *et al.*, “Systemvergleich zwischen Wasserstoffverbrennungsmotor und Brennstoffzelle im schweren Nutzfahrzeug,” *E-Mobil BW GmbH – Landesagentur Für Neue Mobilitätslösungen Automot. Baden-Württ. Stuttg.*, 2021, [Online]. Available: https://www.e-mobilbw.de/fileadmin/media/e-mobilbw/Publikationen/Studien/e-mobilBW-Studie_H2-Systemvergleich.pdf

[10] P. H. Affonso Nóbrega, “A review of physics-based low-temperature proton-exchange membrane fuel cell models for system-level water and thermal management studies,” *J. Power Sources*, vol. 558, p. 232585, Feb. 2023, doi: 10.1016/j.jpowsour.2022.232585.

[11] F. Barbir, *PEM fuel cells: theory and practice*, 2nd ed. Amsterdam ; Boston: Elsevier/Academic Press, 2013.

[12] A. L. Dicks and D. A. J. Rand, *Fuel Cell Systems Explained (3rd Edition)*. John Wiley & Sons, 2018.

[13] M. B. Bertagni, S. W. Pacala, F. Paulot, and A. Porporato, “Risk of the hydrogen economy for atmospheric methane,” *Nat. Commun.*, vol. 13, no. 1, Art. no. 1, Dec. 2022, doi: 10.1038/s41467-022-35419-7.

[14] K. Jiao *et al.*, “Designing the next generation of proton-exchange membrane fuel cells,” *Nature*, vol. 595, no. 7867, Art. no. 7867, Jul. 2021, doi: 10.1038/s41586-021-03482-7.

[15] L. Strandberg, “Electrode Degradation in Proton Exchange Membrane Fuel Cells,” Thesis for the degree of Doctor of Philosophy, Chalmers University of Technology, Gothenburg, Sweden, 2025. [Online]. Available: https://research.chalmers.se/publication/545614

[16] M. Nöst, C. Doppler, M. Klell, and A. Trattner, “Chapter 7 - Thermal Management of PEM Fuel Cells in Electric Vehicles,” in *Comprehensive Energy Management - Safe Adaptation, Predictive Control and Thermal Management*, D. Watzenig and B. Brandstätter, Eds., in SpringerBriefs in Applied Sciences and Technology. , Graz, Austria: Springer International Publishing, 2018, pp. 102–121. doi: 10.1007/978-3-319-57445-5.

[17] J. Ramousse, O. Lottin, S. Didierjean, and D. Maillet, “Heat sources in proton exchange membrane (PEM) fuel cells,” *J. Power Sources*, vol. 192, no. 2, pp. 435–441, Jul. 2009, doi: 10.1016/j.jpowsour.2009.03.038.
[18] Y. Huang, X. Xiao, H. Kang, J. Lv, R. Zeng, and J. Shen, “Thermal management of polymer electrolyte membrane fuel cells: A critical review of heat transfer mechanisms, cooling approaches, and advanced cooling techniques analysis,” *Energy Convers. Manag.*, vol. 254, p. 115221, Feb. 2022, doi: 10.1016/j.enconman.2022.115221.
[19] S. Yu and D. Jung, “Thermal management strategy for a proton exchange membrane fuel cell system with a large active cell area,” *Renew. Energy*, vol. 33, no. 12, Art. no. 12, Dec. 2008, doi: 10.1016/j.renene.2008.02.015.
[20] VDI e. V., Ed., *VDI Heat Atlas*, Second edition. Springer Berlin Heidelberg, 2010. doi: 10.1007/978-3-540-77877-6.
[21] F. P. Incropera, D. P. DeWitt, T. L. Bergman, and A. S. Lavine, Eds., *Fundamentals of heat and mass transfer*, 6. ed. Hoboken, NJ: Wiley, 2007.
[22] C. V. Madhusudana, *Thermal Contact Conductance*. in Mechanical Engineering Series. Cham: Springer International Publishing, 2014. doi: 10.1007/978-3-319-01276-6.
[23] E. Eder, S. Hiller, D. Brüggemann, and M. Preißinger, “Characteristics of air–liquid heat and mass transfer in a bubble column humidifier,” *Appl. Therm. Eng.*, vol. 209, p. 118240, Jun. 2022, doi: 10.1016/j.applthermaleng.2022.118240.
[24] C. Doppler and B. Lindner-Rabl, “Fuel Cell Trucks: Thermal Challenges in Heat Exchanger Layout,” *Energies*, vol. 16, no. 10, Art. no. 10, Jan. 2023, doi: 10.3390/en16104024.
[25] C. Mayer, J. Karner, T. Eberhart, K. Huber, and J. Konrad, “Fuel Cell Electric Tractor FCTRAC: Vehicle Design and Architecture,” *Agric. Eng.*, vol. 79, no. 3, Art. no. 3, Aug. 2024, doi: 10.15150/AE.2024.3315.
[26] M. Wagenblast *et al.*, “Design and Analysis of a Spray Cooling System for a Heavy-Duty Fuel Cell Truck,” *SAE Tech. Pap.*, pp. 2022-01–5054, Jun. 2022, doi: 10.4271/2022-01-5054.
[27] Institution of Mechanical Engineers - IMechE, *Advanced Thermal Management in Future Hydrogen Fuel Cell Powered Vehicles*, (Jun. 13, 2021). Accessed: Jan. 13, 2023. [Online Video]. Available: https://www.youtube.com/watch?v=wol9w7qqKmI
[28] J. Linderl, J. Mayr, M. Hütter, and R. Döbereiner, “Optimized Fuel Cell Drive for Long-haul Trucks,” *ATZheavy Duty Worldw.*, vol. 14, no. 1, pp. 38–43, Mar. 2021, doi: 10.1007/s41321-021-0407-5.
[29] A. Fly, “Thermal and Water Management of Evaporatively Cooled Fuel Cell Vehicles,” Thesis for the degree of Doctor of Philosophy, Loughborough University, Loughborough, England, 2015.
[30] M. Striednig, M. Cochet, P. Boillat, T. J. Schmidt, and F. N. Büchi, “A model based investigation of evaporative cooling for polymer electrolyte fuel cells – Stack level analysis,” *J. Power Sources*, vol. 517, p. 230706, Jan. 2022, doi: 10.1016/j.jpowsour.2021.230706.
[31] R. Prabakaran, M. Mohamed Souby, J. Liu, and S. Chul Kim, “Thermal performance of a stack cooling radiator coupled with spray cooling for the future fuel cell electric vehicles,” *Appl. Therm. Eng.*, vol. 246, p. 122975, Jun. 2024, doi: 10.1016/j.applthermaleng.2024.122975.
[32] D. K. Lee, D. S. Kim, H. S. Byun, H. S. Kang, Y. H. Shin, and H. S. Lee, “Maximizing FCEV Stack Cooling Performance: Developing a Performance Prediction Model Based on Machine Learning for Evaporative Cooling Radiator,” presented at the WCX SAE World Congress Experience, Detroit, Michigan, United States, Apr. 2024, pp. 2024-01–2586. doi: 10.4271/2024-01-2586.
[33] E. J. Choi, J. Y. Park, and M. S. Kim, “Two-phase cooling using HFE-7100 for polymer electrolyte membrane fuel cell application,” *Appl. Therm. Eng.*, vol. 148, pp. 868–877, Feb. 2019, doi: 10.1016/j.applthermaleng.2018.11.103.
[34] M. Reichler, “Theoretische Untersuchungen zur Kühlleistungssteigerung durch innovative Kühlsysteme für Brennstoffzellen-Elektrofahrzeuge,” Abhandlung Doktor-Ingenieur (Dr.-Ing.), Universität Stuttgart, Stuttgart, 2009. [Online]. Available: https://elib.uni-stuttgart.de/server/api/core/bitstreams/6d749339-0633-4f10-a135-a3bbc548069c/content
[35] S. Lee and M. S. Kim, “Stack cooling system coupled with secondary heat pump in fuel cell electric vehicles,” *Energy Convers. Manag.*, vol. 284, p. 116961, May 2023, doi: 10.1016/j.enconman.2023.116961.

[36] S. C. Kim, J. P. Won, Y. S. Park, T. W. Lim, and M. S. Kim, “Performance evaluation of a stack cooling system using CO2 air conditioner in fuel cell vehicles,” *Int. J. Refrig.*, vol. 32, no. 1, pp. 70–77, Jan. 2009, doi: 10.1016/j.ijrefrig.2008.07.003.
[37] S. Swathi, A. S. Oberoi, and R. K. Singla, “Utilizing phase change materials for proton exchange membrane fuel cell cooling: A review,” *Environ. Prog. Sustain. Energy*, p. e14596, Mar. 2025, doi: 10.1002/ep.14596.
[38] N. Philip and P. C. Ghosh, “A generic sizing methodology for thermal management system in fuel cell vehicles using pinch analysis,” *Energy Convers. Manag.*, vol. 269, p. 116172, Oct. 2022, doi: 10.1016/j.enconman.2022.116172.
[39] A. Baroutaji *et al.*, “Advancements and prospects of thermal management and waste heat recovery of PEMFC,” *Int. J. Thermofluids*, vol. 9, p. 100064, Feb. 2021, doi: 10.1016/j.ijft.2021.100064.
[40] L. Guzzella and A. Sciarretta, *Vehicle Propulsion Systems: Introduction to Modeling and Optimization*. Berlin, Heidelberg: Springer Berlin Heidelberg, 2013. doi: 10.1007/978-3-642-35913-2.
[41] K. Popp and W. Schiehlen, *Ground Vehicle Dynamics*. Berlin, Heidelberg: Springer Berlin Heidelberg, 2010. doi: 10.1007/978-3-540-68553-1.
[42] A. Huicochea, R. J. Romero, W. Rivera, G. Gutierrez-Urueta, J. Siqueiros, and I. Pilatowsky, “A novel cogeneration system: A proton exchange membrane fuel cell coupled to a heat transformer,” *Appl. Therm. Eng.*, vol. 50, no. 2, Art. no. 2, Feb. 2013, doi: 10.1016/j.applthermaleng.2011.10.064.
[43] W. Rivera, R. Best, M. J. Cardoso, and R. J. Romero, “A review of absorption heat transformers,” *Appl. Therm. Eng.*, vol. 91, pp. 654–670, Dec. 2015, doi: 10.1016/j.applthermaleng.2015.08.021.
[44] K. E. Herold, R. Radermacher, and S. A. Klein, *ABSORPTION CHILLERS AND HEAT PUMPS*, Second edition. Boca Raton, FL: CRC Press, 2016.
[45] R. G. de Oliveira, “CHEMISORPTION HEAT PUMPS FOR WATER HEATING AND STEAM PRODUCTION,” in *Novel Concepts for Energy-Efficient Water Heating Systems*, Nova Science Publishers, Inc., 2013.
[46] P. Donnellan, K. Cronin, and E. Byrne, “Recycling waste heat energy using vapour absorption heat transformers: A review,” *Renew. Sustain. Energy Rev.*, vol. 42, pp. 1290–1304, Feb. 2015, doi: 10.1016/j.rser.2014.11.002.
[47] Z. Yang, M. Qu, and K. R. Gluesenkamp, “Ammonia-based chemisorption heat pumps for cold-climate heating applications: A comprehensive review,” *Appl. Therm. Eng.*, vol. 179, p. 115674, Oct. 2020, doi: 10.1016/j.applthermaleng.2020.115674.
[48] J. A. Hernández-Magallanes, W. Rivera, and A. Coronas, “Resorption Heat Transformers Operating with the Ammonia- Lithium Nitrate Mixture,” presented at the 12th IEA Heat Pump Conference, Rotterdam: Stichting HPC, 2017.
[49] F. Cudok *et al.*, “Absorption heat transformer - state-of-the-art of industrial applications,” *Renew. Sustain. Energy Rev.*, vol. 141, p. 110757, May 2021, doi: 10.1016/j.rser.2021.110757.
[50] K. Parham, M. Khamooshi, D. B. K. Tematio, M. Yari, and U. Atikol, “Absorption heat transformers – A comprehensive review,” *Renew. Sustain. Energy Rev.*, vol. 34, pp. 430–452, Jun. 2014, doi: 10.1016/j.rser.2014.03.036.